A&A 542, A35 (2012)
DOI: 10.1051/0004-6361/201219215
© ESO 2012

Astronomy & Astrophysics

Na I spectra in the 1.4–14 micron range: transitions and oscillator strengths involving f-, g-, and h-states

S. Civiš[1], M. Ferus[1], P. Kubelík[1], P. Jelinek[1], V. E. Chernov[1,2], and E. M. Zanozina[3,1]

[1] J. Heyrovský Institute of Physical Chemistry, Academy of Sciences of the Czech Republic, Dolejškova 3, 18223 Prague 8, Czech Republic
e-mail: civis@jh-inst.cas.cz
[2] Voronezh State University, 394693 Voronezh, Russia
[3] State Research Center of Russian Federation Troitsk Institute of Innovation and Fusion Research, 142190 Troitsk, Moscow Region, Russia

Received 13 March 2012 / Accepted 24 April 2012

ABSTRACT

Context. Compared with the visible and ultraviolet ranges, fewer atomic and ionic lines are available in the infrared spectral region. Atlases of stellar spectra often provide only a short list of identified lines, and modern laboratory-based spectral features for wavelengths longer than 1 micron are not available for most elements. For the efficient use of the growing capabilities of infrared (IR) astronomy, detailed spectroscopical information on atomic line features in the IR region is needed.

Aims. Parts of the infrared stellar (e.g., solar) spectra in the 1200–1800 cm^{-1} (5.6–8 μm) range have never been observed from the ground because of heavy contamination of the spectrum by telluric absorption lines. Such an infrared spectrum represents a great challenge for laboratory observations of new, unknown infrared atomic transitions involving the atomic levels with high orbital momentum and their comparison with the available spectra.

Methods. The vapors of excited Na I atoms are produced during the ablation of the salt (sodium iodide, Na I) targets by a high-repetition rate (1.0 kHz) pulsed nanosecond ArF laser ExciStar S-Industrial V2.0 1000, pulse length 12 ns, λ = 193 nm, output energy of 15 mJ, fluence about 2–20 J/cm^2 inside a vacuum chamber (average pressure 10^{-2} Torr). The time-resolved emission spectrum of the neutral atomic potassium (Na I) was recorded in the 700–7000 cm^{-1} region using the Fourier transform infrared spectroscopy technique with a resolution of 0.02 cm^{-1}. The f-values calculated in the quantum-defect theory approximation are presented for the transitions involving the reported Na I levels.

Results. This study reports precision laboratory measurements for 26 Na I lines in the range of 700–7000 cm^{-1} (14–1.4 μm), including 20 lines not measured previously in the laboratory. This results in newly observed 7h, 6h, and 6g levels, and improved energy determination for ten previously known levels. The doublet structure of the 4f level has been observed for the first time. For transitions between the observed levels, we report calculated f-values that agree reasonably well with experiment.

Conclusions. The recorded Na I line features agree with the data from the available solar spectrum atlases. The energy values of Na I 4s, 4p, 5p, 6p, 4f, 5f, and 5g levels extracted from our spectra have lower uncertainties as compared to the values reported several decades ago, but the latter values slightly differ from ours.

Key words. atomic data – line: identification – techniques: spectroscopic – Sun: infrared

1. Introduction

There are several reasons why the spectra of neutral sodium are of astrophysical importance. For instance, in studying the galactic fountain process (gas flows from the disk of galaxies produced by multiple supernova explosions which play an important role in formation of high, and intermediate-velocity clouds, see Spitoni et al. 2008), Na I is a good tracer for a neutral gas because of its low first ionization potential (5.1 eV). Na I absorption is expected to be observed in the inflow (the later) stage of the galactic fountain process when the gas is mostly neutral, and nearly absent during the outflow (the earlier) stage when the gas is believed to be almost fully ionized. The sodium enrichment of supergiant atmospheres is one of the long-standing problems in observational stellar astrophysics (Andrievsky et al. 2002). The overabundance of Na in the atmospheres of F, G, K supergiants is in a correlation with the stellar mass. The high probability of emissions of Na I at visible wavelengths makes its detection easy to use in studies of the exospheres (the outermost atmospheric layers) of some solar system bodies, e.g., Mercury (Mouawad et al. 2011), the Moon (Matta et al. 2009; Lee et al. 2011) and Io (Grava et al. 2010). Na I has also been identified in exoplanetary atmospheres (Jensen et al. 2011) through space-based, from onboard the *Hubble* Space Telescope (Charbonneau et al. 2002) and ground-based, the *Hobby-Eberly* Telescope (Redfield et al. 2008), observations.

The detection of neutral sodium in the aforementioned examples was performed at optical wavelengths. The sodium enrichment of the atmospheres of 48 supergiants and bright giants and its connection with stellar gravity was studied using two Na I lines, 6154 and 6160 Å (Andrievsky et al. 2002). The observations of time-variable Na I absorption features near the resonance doublet (D lines at 589 nm) in circumstellar matter are used for the investigation of evolution models of type Ia supernova progenitors (Sternberg et al. 2011). The Na I emission at the resonance doublet recorded by MESSENGER's Mercury Atmospheric and Surface Composition Spectrometer (MASCS) was used to constrain models of Mercury's sodium

exosphere (Mouawad et al. 2011). The measured Na I absorption near the resonance doublet in the transmission spectrum of an extrasolar planet (Charbonneau et al. 2002) showed large discrepancies with models that used a solar abundance of atomic sodium in planetary atmosphere. The amount of absorption of Na I for other planets differs significantly (Redfield et al. 2008), which indicates that the two exoplanets may have significantly different atmospheric properties, in particular the temperature profiles of their atmospheres. A direct measurement of the effective temperature of the planetary atmospheres and confirmation of a thermal inversion therein could be provided by exploiting the enhanced contrast between stars and their planets in the infrared wavelengths (O'Donovan et al. 2010).

The infrared (IR) range is becoming more and more important in astronomical research. Recent research topics include studies of dust-obscured objects and interstellar clouds, cool objects such as dwarfs, disks or planets, and the extended atmospheres of evolved stars, including objects at cosmological distances from the Earth (Kerber et al. 2009). The great advantages of Fourier transform infrared spectroscopy (FTIR), such as its constant high resolution and energy throughput, have made the IR spectral region more accessible for laboratory spectral measurements (Nilsson 2009).

However, compared with the visible and ultraviolet ranges, fewer atomic and ionic lines are available in the IR spectral region (Ryde 2010). Atlases of stellar spectra often provide only a short list of identified lines (Lobel 2011), and modern laboratory-based spectral features for wavelengths longer than 1 micron are not available for most elements (Wahlgren 2011). The powerful capabilities of IR astronomy cannot be fully utilized without detailed spectroscopical information on atomic line features in the IR region, in particular, wavelengths and oscillator strengths (Biémont 1994; Grevesse & Noels 1994; Pickering 1999; Jorissen 2004; Johansson 2005; Pickering et al. 2011).

New laboratory spectra may identify spectral lines in the IR that could result in the discovery of new excited atomic levels that are difficult to compute accurately and must be determined solely from IR lines (Wahlgren 2011). Including additional energy levels, atomic transition lines and oscillator strengths will increase the reliability of astrophysical calculations such as stellar or planetary atmosphere models.

Na I at 7880 cm^{-1} (1.269 μm) first appears in early G spectral type stars and grows in strength toward later types (Wallace et al. 2000). The near-infrared line list (with oscillator strengths computed or obtained by fitting the solar spectrum) for Na I includes the 10 182–12 679 and 16 374–16 389 cm^{-1} (0.98186–0.78849 and 0.61056–0.60999 μm) ranges (Meléndez & Barbuy 1999). Some Na I lines are identified in the solar spectrum in Atmospheric Chemistry Experiment with a space-borne Fourier transform spectrometer (ACE-FTS), which has been performed onboard a SCISAT-1 satellite (Hase et al. 2010). The ACE solar atlas covers the 700–4430 cm^{-1} (14.3–2.26) range at a resolution of 0.02 cm^{-1}. The measurements performed with FTS at the McMath-Pierce solar telescope (National Solar Observatory, Kitt Peak) cover the range 460–13600 cm^{-1} (22–0.74 μm), performed with some corrections to account for telluric absorption (Wallace et al. 1996). Parts of the IR range in 1200–1800 cm^{-1} (8–5.6 μm) have never been observed from the ground due to heavy contamination of the spectrum by telluric absorption lines. Such an infrared spectrum represents a great challenge for laboratory observations of new, unknown infrared atomic transitions involving the atomic levels with high orbital momentum (Civiš et al. 2011a) and their comparison with the available stellar (e.g., solar) spectra. An attempt to fill this gap for Na I is made in the present paper.

Since the middle of the past century, when the measurements of the Na I spectrum were performed by Risberg (1956) in the range of 0.737–1.14 μm (13 559–8767 cm^{-1}) and by Johansson (1961) in the range of 1.2–3.0 μm (7885–4276 cm^{-1}), only one neutral sodium IR line (4f–5g transition at 2472.622 cm^{-1} i.e. 4.04319 μm) has been reported (Litzen 1970). In this hollow-cathode measurement no lines with longer wavelengths were recorded, and no emissions from ng (with $n > 5$) nor nh-levels were observed. The energies of the ng and nh levels of Na I for $6 \leq n \leq 13$ available in the NIST database (Ralchenko et al. 2010) or critical compilations (Sansonetti 2008) are calculated by extrapolation from the higher nh and ng levels with $n \geq 13$ (Dyubko et al. 1997). They have never been measured experimentally. The f-values for the Na I transitions listed in the NIST database and critical compilations (Kelleher & Podobedova 2008) are taken from the very old measurements by Filippov & Prokofjew (1929) (taken before the rise of quantum mechanics) or from multi-configuration Dirac-Hartree-Fock calculations using the code by Froese Fischer (2002).

Here we report the results of an FTIR spectroscopy study of Na I transitions in four IR ranges: 1.4–2.5, 2.7–5.0, 5.9–9.1 and 11.1–14.3 μm. From the recorded spectra, we extracted the excitation energies of the 7h, 6h, and 6g states of Na I for which only theoretical predictions were previously avaible. In addition, we also calculated f-values for all transitions involving the observed Na I levels using quantum-defect theory (QDT) approximation. Comparisons with measured transition probabilities and oscillator strengths (Miculis & Meyer 2005; Nawaz et al. 1992) indicate that the QDT is a suitable approximation.

2. Methods

Transitions in the four IR spectra ranges defined previously can be observed using laser-induced breakdown spectroscopy (LIBS), which analyzes the light spectrum emitted from plasma created on the sample surface by laser pulses (laser ablation). Laser ablation is a versatile and sensitive probe for the detection and identification of trace substances. As such, this technique has many practical advantages over the conventional chemical analysis methods (Aragon & Aguilera 2008; Lednev & Pershin 2008) and is being used in a growing number of applications (Lee et al. 2004; Babánková et al. 2006; Gomes et al. 2004; Barthélemy et al. 2005; Aragon & Aguilera 2008). In this study, we combined LIBS with time-resolved Fourier-transform infrared (FTIR) spectroscopy to record IR emission spectra in seven spectral ranges: 800–1000, 1000–1300, 1200–1600, 1600–2000, 2000–3500, 4100–5000, and 5000–7700 cm^{-1} (12.5–10, 10–7.7, 8.33–6.25, 6.25–5.0, 5.0–2.85, 2.34–2.0, 2.0–1.3 μm). Note that measurements in the range below 1800 cm^{-1} ($\lambda > 5.55$ μm) are quite difficult because of the low sensitivity of the mercury-cadmium-telluride (MCT) detector and the high background (blackbody) radiation level. To our knowledge, there are no laboratory-measured spectra of alkali metals below 1800 cm^{-1}. All the wavenumbers listed in the NIST database (Ralchenko et al. 2010) for the alkali metal atomic lines below 1800 cm^{-1} are Ritz wavenumbers (i.e., obtained by subtracting known energy level values, not from laboratory-measured spectra). Below we briefly describe the experimental setup used in the present work. For more details see our previous papers (Kawaguchi et al. 2008; Civiš et al. 2010; Civiš et al. 2011b).

Table 1. Observed Na lines and their identification.

Present work						Other measurements		
Wavenumber (cm^{-1})	Air wavelengths (μm)	log(I)	SNR	HWHM (cm^{-1})	Identification	NIST (Sansonetti 2008)	ACE (Hase et al. 2010)	NSO (Wallace et al. 1996)
808.786 ± 0.004	12.3608	4.60	3.6	0.070 ± 0.009	6g–7h			
925.012 ± 0.011	10.8077	4.33	5.5	0.064 ± 0.037	$6s_{\frac{1}{2}}$–$6p_{\frac{3}{2}}$			
1094.097 ± 0.006	9.137466	3.73	9.5	0.048 ± 0.021	$3d_{\frac{3}{2}}$–$4p_{\frac{1}{2}}$		1094.102	
1099.744 ± 0.003	9.090547	4.11	27.	0.063 ± 0.008	$3d_{\frac{5}{2}}$–$4p_{\frac{3}{2}}$		1099.746	
1329.751 ± 0.008	7.518155	3.28	6.3	0.061 ± 0.029	$5p_{\frac{3}{2}}$–$6s_{\frac{1}{2}}$		1329.765	
1332.218 ± 0.013	7.504233	3.48	3.1	0.090 ± 0.045	$5p_{\frac{1}{2}}$–$6s_{\frac{1}{2}}$		1332.240	
1341.651 ± 0.003	7.451472	3.94	15.	0.091 ± 0.009	5g–6h		1341.677	
1343.194 ± 0.009	7.442912	3.55	7.4	0.095 ± 0.027	5f–6g		1343.246	
1839.707 ± 0.003	5.434166	6.23	22.	0.097 ± 0.010	$5s_{\frac{1}{2}}$–$5p_{\frac{1}{2}}$		1839.707	
1842.185 ± 0.002	5.426857	6.51	32.	0.105 ± 0.008	$5s_{\frac{1}{2}}$–$5p_{\frac{3}{2}}$		1842.183	
1993.867 ± 0.007	5.014012	6.25	9.4	0.162 ± 0.021	$5p_{\frac{3}{2}}$–$5d_{\frac{5}{2}}$		1993.856	
1996.353 ± 0.010	5.007769	5.93	7.9	0.133 ± 0.031	$5p_{\frac{1}{2}}$–$5d_{\frac{3}{2}}$		1996.369	
2150.197 ± 0.009	4.649469	1.86	3.9	0.047 ± 0.052	5g–7h		2150.336	
2472.603 ± 0.002	4.043218	3.75	40.	0.119 ± 0.006	4f–5g	2472.620 ± 0.010	2472.612	2472.62
2508.928 ± 0.003	3.984679	3.34	26.	0.127 ± 0.008	$4d_{\frac{5}{2}}$–$5f_{\frac{7}{2}}$		2508.927	2508.94
2928.083 ± 0.003	3.414272	3.07	27.	0.111 ± 0.009	$4p_{\frac{3}{2}}$–$5s_{\frac{1}{2}}$		2928.086	
2933.671 ± 0.004	3.407769	2.72	18.	0.096 ± 0.014	$4p_{\frac{1}{2}}$–$5s_{\frac{1}{2}}$		2933.682	
2969.160 ± 0.013	3.367038	2.74	4.5	0.104 ± 0.043	$5p_{\frac{3}{2}}$–$7s_{\frac{1}{2}}$		2969.179	
3344.378 ± 0.005	2.989277	3.49	13.	0.109 ± 0.016	$5p_{\frac{3}{2}}$–$6d_{\frac{5}{2}}$		3344.365	
3346.866 ± 0.006	2.987055	3.20	11.	0.112 ± 0.019	$5p_{\frac{1}{2}}$–$6d_{\frac{3}{2}}$		3346.820	
4276.126 ± 0.003	2.337927	5.76	5.1	0.178 ± 0.012	$4p_{\frac{3}{2}}$–$4d_{\frac{5}{2}}$	4276.150 ± 0.005	4276.132	4276.151
4281.759 ± 0.004	2.334851	5.24	11.	0.106 ± 0.011	$4p_{\frac{1}{2}}$–$4d_{\frac{3}{2}}$	4281.784 ± 0.006	4281.756	4281.776
4526.968 ± 0.002	2.208381	6.11	13.	0.160 ± 0.006	$4s_{\frac{1}{2}}$–$4p_{\frac{1}{2}}$	4526.999 ± 0.006		4526.999
4532.568 ± 0.001	2.205653	6.35	25.	0.152 ± 0.004	$4s_{\frac{1}{2}}$–$4p_{\frac{3}{2}}$	4532.594 ± 0.006		4532.589
5414.005 ± 0.003	1.846557	5.22	1.3	0.089 ± 0.020	$3d_{\frac{3}{2}}$–$4f_{\frac{5}{2}}$	5414.058 ± 0.009		
5414.063 ± 0.002	1.846537	5.35	1.8	0.096 ± 0.015	$3d_{\frac{5}{2}}$–$4f_{\frac{7}{2}}$	5414.058 ± 0.009		

Notes. Each of the seven spectral ranges has its own scale of arbitrary units for the emission intensity, I, which are given logarithmically. The uncertainties of the other measurements are 0.001 cm^{-1} (ACE) and 0.008–0.015 cm^{-1} (NSO).

The vapors of excited Na atoms are produced during the ablation of the salt (Na I) targets by a high-repetition rate (1.0 kHz) pulsed nanosecond ArF laser (ExciStar S-Industrial V2.0 1000, pulse length 12 ns, λ = 193 nm, output energy of 15 mJ, fluence about 2–20 J/cm^2) inside a vacuum chamber (average pressure 10^{-2} Torr). The time resolution FTIR spectra were measured using the Bruker IFS 120 HR spectrometer. For the 2000–7700 cm^{-1} (1.3–5.0 μm) range we used a CaF_2 beam splitter and an InSb detector, while for the 700–2000 cm^{-1} range, a KBr beam splitter and an HgCdTe (MCT) detector were used. The infrared emission (axial distance from the target approximately 10 mm) was focused into the spectrometer using a CaF_2 or ZnSe lens (for 2000–7700 cm^{-1} (1.3–5.0 μm) or 700–2000 cm^{-1} (14.3–5.0 μm) respectively). The wavenumbers, line widths and their intensities (as well as the uncertainties for these quantities) are presented in Table 1.

For data sampling, we used the so-called 1/3-sampling (Civiš et al. 2010), where the scanner velocity was set to produce a 3 kHz He–Ne laser interference signal, and the ArF laser oscillation was triggered at one third of the He-Ne frequency. Measurements were performed with a resolution of 0.017 cm^{-1}, and three scans were needed to complete the interferogram. The resolution of 0.017 cm^{-1} allows us to collect 64 time-shifted interferograms. At higher resolutions, the number of interferograms was reduced to 30. Higher spectral resolution requires a longer scanning time, an increase in the number of laser pulses (the lifetime of the ArF excimer laser is limited by the total number of pulses) and a reduction of the entrance aperture of the spectrometer (fewer photons on the detector).

Usually, 3 to 30 scans were coadded to obtain a reasonable signal-noise ratio. The acquired spectrograms were post-zero filled by a factor of 2 and analyzed using a commercial software routine (Bruker OPUS Ver.3.1) (OPUS 2010). Finally, the spectra were corrected by subtracting the blackbody background spectrum.

Using a time-resolved scheme is essential, because the emission intensities of the spectra lines are dependent on the time delay after the ArF laser pulse shot. The time profiles of the emission lines have maxima at different delay times $\tau \simeq 10...20$ μs after a laser shot. This non-monotonic decay of the emission intensity could be due to a complex combination of the repopulation of the atomic Na states by collisional cascade (Civiš et al. 2010) and the transfer processes in ablation products (Khalil & Sreenivasan 2005; Kawaguchi et al. 2008).

For an optically thin plasma at local thermal equilibrium (LTE), the emission transition from an upper state k to a

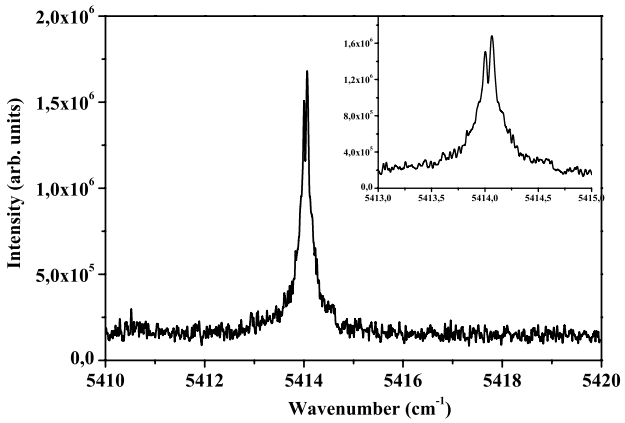

Fig. 1. Resolved fine structure of the 3d–4f transition.

lower state i has the intensity I_{ki} proportional to the transition probability A_{ki} and to the transition wavenumber ν_{ki}:

$$I_{ki} \sim g_k A_{ki} \nu_{ki} \exp\left(-\frac{E_k}{k_B T}\right), \quad (1)$$

where k_B is the Boltzmann constant, T is the excitation temperature, E_k and g_k being the energy and the degeneracy factor of the upper state, respectively. Since at the low pressures, used in our experiment the atom concentration is low, we can consider our plasma to be optically thin. However, in the same conditions some deviations from LTE conditions can occur, see Giacomo et al. (2001), but the Boltzmann distribution of the atomic populations remains valid according to Qi et al. (2007), although with different temperatures of electrons and atoms, see Giacomo et al. (2001). This means that even if the observed line intensities slightly deviate from the proportionality to the A-values, they should describe the qualitative picture of the relative line intensities well enough to assign the lines. The dipole matrix elements required to determine A_{ki} were calculated using the single-channel quantum defect theory (QDT) (Chernov et al. 2000, 2005a).

3. Results and discussion

A list of the observed lines with their parameters and identification is presented in Table 1. The measurements were performed in the seven spectral ranges mentioned in Sect. 2. Only lines within the same spectral range have intensities with the same scale. Eighteen lines in Table 1 have not previously been measured in laboratories. Also, note that we have resolved the fine structure of the 3d–4f transition, see Fig. 1.

Table 1 also contains the wavenumbers of some Na I lines as measured in laboratories (Litzen 1970; Johansson 1961), by a ground-based (McMath-Pierce solar telescope at Kitt Peak; Wallace et al. 1996) and space-based (ACE; Hase et al. 2010) Fourier transform spectrometers. The uncertainty of ACE peak picking is 0.001 cm^{-1}, which is less than our technique. The accuracy of the National Solar Observatory wavenumbers (Wallace et al. 1996) can be evaluated from the resolving power R = 300 000; the uncertainty $\Delta\nu$ = 0.008–0.015 cm^{-1} for ν = 2400–4500 cm^{-1} (4.16–2.22 μm) is somewhat greater than uncertainties given in Table 1. However, for several lines our uncertainties are better than previous laboratory measurements, 0.005 cm^{-1} in (Johansson 1961) and 0.01 cm^{-1} in (Litzen 1970). Our wavenumbers agree with these laboratory measurements

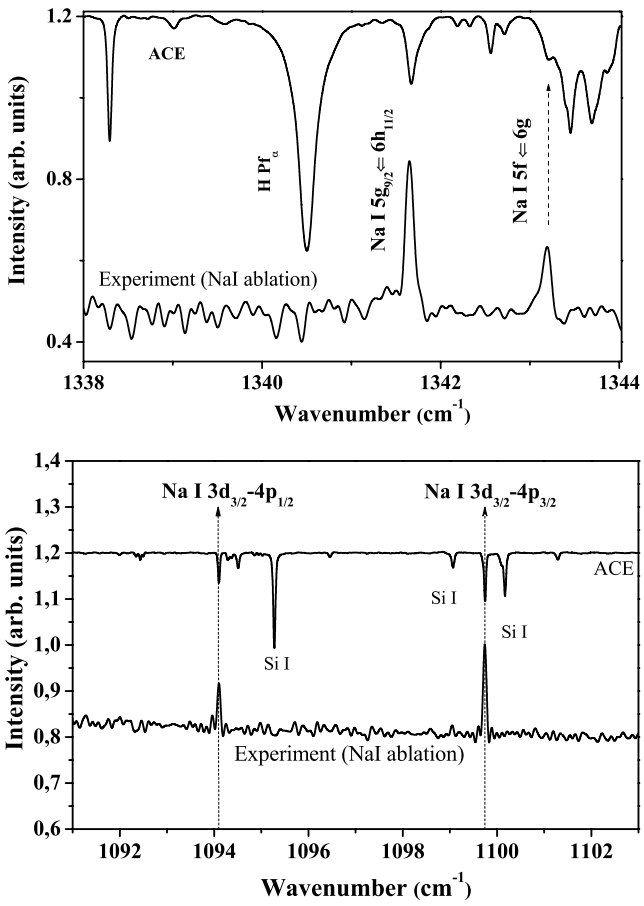

Fig. 2. Emission spectra from Na I ablation plasma and the ACE (Hase et al. 2010) solar spectra.

within the uncertainties, but the measurements do not always coincide with the wavenumbers listed in the ACE and NSO atlases.

The ACE-FTS spectral data are represented as three data lists. The second data list (according to Hase et al. 2010) contains the set of wavenumbers and transitions specified in the graphic ACE atlas pages. A simple analysis shows that the Na I line wavenumbers encountered in data list 2 are simply the Ritz wavenumbers obtained from the Na I level energies stored in the NIST database (Ralchenko et al. 2010). The first data list is presented in two variants: (a) the list of observed lines and (b) the corrected (by an empirical calibration factor of 1.00000294) version of the observed data; the correction was made to achieve closer agreement with the line positions specified in the second data list. We consider the ACE data list 1 (uncorrected) to be the most relevant to compare with our results since the above correction (by a calibration factor of 1.00000294) was performed in the ACE atlas (Hase et al. 2010) to aid the assignment of the spectral signatures in the ACE solar spectrum with the line positions given in current spectroscopic line-lists.

The largest discrepancies occur for the lines corresponding to transitions from high-l levels (5g, 6g, 6h, 7h). These discrepancies could be explained by the Stark shift of solar lines due to high (up to 1000 V cm^{-1}) electric fields in the Sun's atmosphere. For instance, Mg I solar lines in the range of 7–12 μm (corresponding to transitions from nl levels with $n, l \geq 6$) can differ from laboratory measurements by −0.01 to +0.03 cm^{-1} (Chang & Schoenfeld 1991). The quadratic Stark effect is determined

Table 2. Improved energy measurements (cm^{-1}) of several Na I levels.

Level	Present work	Other sources
7h	39 209.670 ± 0.015	[39 209.887 ± 0.002] (Dyubko et al. 1997)
6h	38 401.144 ± 0.012	[38 401.147 ± 0.002] (Dyubko et al. 1997)
6g	38 400.865 ± 0.015	[38 400.904 ± 0.002] (Dyubko et al. 1997)
$6d_{\frac{3}{2}}$	38 387.266 ± 0.002	38 387.268 ± 0.002 (Martin & Zalubas 1981; Juncar et al. 1981)
$6d_{\frac{5}{2}}$	38 387.252 ± 0.002	38 387.255 ± 0.002 (Martin & Zalubas 1981; Juncar et al. 1981)
$7s_{\frac{1}{2}}$	38 012.022 ± 0.016	38 012.042 ± 0.002 (Martin & Zalubas 1981; Juncar et al. 1981)
$6p_{\frac{3}{2}}$	37 297.622 ± 0.021	37 297.61 ± 0.02 (Risberg 1956)
5g	37 059.497 ± 0.011	37 059.54 ± 0.07 (Litzen 1970)
$5f_{\frac{7}{2}}$	37 057.658 ± 0.007	37 057.65 ± 0.02 (Risberg 1956)
$5d_{\frac{3}{2}}$	37 036.740 ± 0.013	37 036.772 ± 0.002 (Martin & Zalubas 1981; Juncar et al. 1981)
$5d_{\frac{5}{2}}$	37 036.729 ± 0.010	37 036.752 ± 0.002 (Martin & Zalubas 1981; Juncar et al. 1981)
$6s_{\frac{1}{2}}$	36 372.610 ± 0.013	36 372.618 ± 0.002 (Martin & Zalubas 1981; Juncar et al. 1981)
$5p_{\frac{3}{2}}$	35 042.862 ± 0.006	35 042.85 ± 0.02 (Risberg 1956)
$5p_{\frac{1}{2}}$	35 040.387 ± 0.006	35 040.38 ± 0.02 (Risberg 1956)
$4f_{\frac{7}{2}}$	34 586.897 ± 0.007	34 586.92 ± 0.02 (Johansson 1961)
$4f_{\frac{5}{2}}$	34 586.893 ± 0.005	34 586.92 ± 0.02 (Johansson 1961)
$4d_{\frac{3}{2}}$	34 548.761 ± 0.002	34 548.764 ± 0.002 (Martin & Zalubas 1981; Juncar et al. 1981)
$4d_{\frac{5}{2}}$	34 548.726 ± 0.003	34 548.729 ± 0.002 (Martin & Zalubas 1981; Juncar et al. 1981)
$5s_{\frac{1}{2}}$	33 200.673 ± 0.003	33 200.673 ± 0.002 (Martin & Zalubas 1981; Juncar et al. 1981)
$4p_{\frac{3}{2}}$	30 272.586 ± 0.002	30 272.58 ± 0.02 (Risberg 1956)
$4p_{\frac{1}{2}}$	30 266.991 ± 0.003	30 266.99 ± 0.02 (Risberg 1956)
$3d_{\frac{3}{2}}$	29 172.888 ± 0.002	29 172.887 ± 0.002 (Martin & Zalubas 1981; Juncar et al. 1981)
$3d_{\frac{5}{2}}$	29 172.837 ± 0.003	29 172.837 ± 0.002 (Martin & Zalubas 1981; Juncar et al. 1981)
$4s_{\frac{1}{2}}$	25 740.013 ± 0.002	25 739.999 ± 0.003 (Arqueros 1988)

by the polarizability. Even in its ground state, the polarizability of Na I is twice as high as that of Mg in its first excited state (Chernov et al. 2005a,b). Therefore, the wavenumbers of the high-l Na solar lines can differ from their laboratory values by more than 0.03 cm^{-1}, explaining the discrepancies in Table 1. Improved atomic spectra measurements of transitions from the high-l levels, below 2000 cm^{-1} ($\lambda > 5$ μm), may yield more precise solar electric field strengths.

New laboratory spectroscopic measurements are important for a proper interpretation of current and future astrophysical spectra in the IR domain. Measured spectra and ACE-FTS solar spectra in the vicinity of the most prominent lines are shown in Fig. 2.

The energies, E_k, of the levels involved in the corresponding transitions can be extracted from the measured ν_{ki} values. For this refinement we used a least-squares fitting algorithm that is similar to the one proposed by Radziemski et al. (1972). To obtain the best estimates for the level energy values E_k, we performed a minimization of a sum of deviations not only between $E_k - E_j$ and the measured wavenumbers, but also included the deviations between some E_k and the "reference" values for these levels taken from Ralchenko et al. (2010) and Litzen (1970). The weights in the sum of squared deviations were proportional to the inverse uncertainties of the corresponding wavenumbers or "reference" energies. These revised values, together with the new h-level energies, are presented in Table 2.

For most of the observed levels, the extracted E_k agrees with the calculated uncertainties using the level values given by the NIST database and compilation tables (Ralchenko et al. 2010; Sansonetti 2008). The exceptions are the 5d and 7s levels. The slight disagreement with previous works (Martin & Zalubas 1981; Juncar et al. 1981) can be caused by uncertainties in the wavenumbers of the lines involving these levels (as compared to other lines listed in Table 1). Our energies for the nd levels (with $n = 3, 4, 6$) and ns levels (with $n = 5, 6$) agree with the higher precision values measured in previous works (Martin & Zalubas 1981; Juncar et al. 1981). For the 4s, 4p, 5p, 6p, 4f, 5f and 5g levels, we report more accurate energies than previous measurements (Risberg 1956; Johansson 1961; Litzen 1970; Arqueros 1988).

The energies of the 7h, 6h, and 6g levels, given in square brackets in Table 2, have not been measured before. However, theoretical predictions based on extrapolation from the higher nh and ng levels with $n \geq 13$ (Dyubko et al. 1997) were available. Our spectral resolution does not allow us to resolve the fine structure of the h and g levels. The fine splitting of these levels should be less than the nf-levels, which generally decreases with n and is resolved here only for $n = 4$. This fine splitting (~0.06 cm^{-1}) is clearly observed in our spectra (see inset in Fig. 1).

To check the adequacy of the QDT calculations, we compared the dipole matrix elements calculated using QDT with other experimental and calculated values. Although all these dipole matrix elements (f- or A-values) can be easily expressed through each other, we kept the original data of the sources being compared (A-values for 3p–ns, nd transitions and f-values for 3s–np transitions).

Table 3 compares the probabilities (A-values) for the $3p_{\frac{3}{2}}$–$ns_{\frac{1}{2}}$, $nd_{\frac{3}{2}}$ transitions with model potential calculations (modified Coulomb approximation) (Miculis & Meyer 2005) and NIST data (obtained from Dirac-Hartree-Fock, Froese Fischer 2002; or the R-matrix, Taylor 1995, theory). The Dirac-Hartree-Fock calculations differ from our QDT results by not more than 6%. The NIST A-values for $n < 8$ are closer to our values. For higher n, the QDT approximation should give more adequate results than the Dirac-Hartree-Fock calculations.

Table 3. Comparison of probabilities (A-values) for several $3p_{\frac{3}{2}}$–$ns_{\frac{1}{2}}$, $nd_{\frac{3}{2}}$ transitions in Na I with the NIST database values (Ralchenko et al. 2010).

Transition	Present work	Calculation [1]	NIST
$3p_{\frac{3}{2}}$–$4s_{\frac{1}{2}}$	1.68E+7	1.78E+7	1.76E+7 [2]
$3p_{\frac{3}{2}}$–$3d_{\frac{3}{2}}$	8.31E+6	8.58E+6	8.57E+6 [2]
$3p_{\frac{3}{2}}$–$5s_{\frac{1}{2}}$	4.79E+6	5.07E+6	4.98E+6 [2]
$3p_{\frac{3}{2}}$–$4d_{\frac{3}{2}}$	1.98E+6	2.02E+6	2.02E+6 [2]
$3p_{\frac{3}{2}}$–$6s_{\frac{1}{2}}$	2.18E+6	2.31E+6	2.27E+6 [2]
$3p_{\frac{3}{2}}$–$5d_{\frac{3}{2}}$	7.99E+5	8.15E+5	
$3p_{\frac{3}{2}}$–$7s_{\frac{1}{2}}$	1.19E+6	1.26E+6	1.23E+6 [2]
$3p_{\frac{3}{2}}$–$6d_{\frac{3}{2}}$	4.08E+5	4.16E+5	4.14E+5 [2]
$3p_{\frac{3}{2}}$–$8s_{\frac{1}{2}}$	7.21E+5	7.66E+5	7.50E+5 [2]
$3p_{\frac{3}{2}}$–$7d_{\frac{3}{2}}$	2.39E+5	2.43E+5	2.44E+5 [2]
$3p_{\frac{3}{2}}$–$9s_{\frac{1}{2}}$	4.70E+5	5.00E+5	5.61E+5 [2]
$3p_{\frac{3}{2}}$–$8d_{\frac{3}{2}}$	1.52E+5	1.55E+5	1.95E+5 [2]
$3p_{\frac{3}{2}}$–$10s_{\frac{1}{2}}$	3.24E+5	3.44E+5	6.50E+5 [2]
$3p_{\frac{3}{2}}$–$9d_{\frac{3}{2}}$	1.03E+5	1.14E+5	
$3p_{\frac{3}{2}}$–$11s_{\frac{1}{2}}$	2.33E+5	2.47E+5	
$3p_{\frac{3}{2}}$–$10d_{\frac{3}{2}}$	7.38E+4	7.50E+4	7.80E+4 [3]
$3p_{\frac{3}{2}}$–$12s_{\frac{1}{2}}$	1.73E+5	1.84E+5	
$3p_{\frac{3}{2}}$–$11d_{\frac{3}{2}}$	5.44E+4	5.54E+4	
$3p_{\frac{3}{2}}$–$13s_{\frac{1}{2}}$	1.32E+5	1.40E+5	
$3p_{\frac{3}{2}}$–$12d_{\frac{3}{2}}$	4.13E+4	4.20E+4	
$3p_{\frac{3}{2}}$–$14s_{\frac{1}{2}}$	1.03E+5	1.09E+5	
$3p_{\frac{3}{2}}$–$13d_{\frac{3}{2}}$	3.22E+4	3.26E+4	
$3p_{\frac{3}{2}}$–$15s_{\frac{1}{2}}$	8.17E+4	8.70E+4	
$3p_{\frac{3}{2}}$–$14d_{\frac{3}{2}}$	2.56E+4	2.59E+4	
$3p_{\frac{3}{2}}$–$16s_{\frac{1}{2}}$	6.60E+4	7.03E+4	
$3p_{\frac{3}{2}}$–$15d_{\frac{3}{2}}$	2.07E+4	2.09E+4	
$3p_{\frac{3}{2}}$–$17s_{\frac{1}{2}}$	5.41E+4	5.76E+4	
$3p_{\frac{3}{2}}$–$16d_{\frac{3}{2}}$	1.69E+4	1.71E+4	
$3p_{\frac{3}{2}}$–$18s_{\frac{1}{2}}$	4.49E+4	4.78E+4	
$3p_{\frac{3}{2}}$–$17d_{\frac{3}{2}}$	1.41E+4	1.42E+4	
$3p_{\frac{3}{2}}$–$19s_{\frac{1}{2}}$	3.77E+4	4.01E+4	
$3p_{\frac{3}{2}}$–$18d_{\frac{3}{2}}$	1.18E+4	1.19E+4	
$3p_{\frac{3}{2}}$–$20s_{\frac{1}{2}}$	3.19E+4	3.40E+4	
$3p_{\frac{3}{2}}$–$19d_{\frac{3}{2}}$	1.00E+4	1.01E+4	
$3p_{\frac{3}{2}}$–$20d_{\frac{3}{2}}$	8.55E+3	8.62E+3	

Notes. The latter are taken from Miculis & Meyer (2005) if not otherwise stated.

References. [1] Model potential (modified Coulomb approximation (Miculis & Meyer 2005); [2] Dirac-Hartree-Fock calculations (Froese Fischer 2002); [3] close-coupled calculations by R-matrix method (Taylor 1995).

For some 3s–np transitions only the multiplet f-values (i.e., summed over the fine structure components) were measured using laser-based Faraday rotation spectroscopy (Nawaz et al. 1992). We compare the multiplet f-values with the NIST database and our calculations in Table 4. For $n < 17$ our calculations agree well (1–5%) with the laser-based Faraday rotation spectroscopy measurements (Nawaz et al. 1992) while for $n = 18$ the difference is about 19%. The NIST values are taken from quite old measurement by Filippov & Prokofjew (1929).

Table 4. Multiplet f-values of Na I.

Transition	Present work	Experiment [1]	NIST
3s–9p	8.246E-5	8.110E-5	8.98E-5 [2], [3]
3s–10p	5.210E-5	5.322E-5	5.28E-5 [2]
3s–11p	3.563E-5	3.614E-5	5.35E-5 [2], [4]
3s–12p	2.449E-5	2.545E-5	3.93E-5 [2], [4]
3s–13p	1.946E-5	1.867E-5	3.04E-5 [2], [4]
3s–14p	1.427E-5	1.421E-5	2.27E-5 [2], [4]
3s–15p	1.143E-5	1.102E-5	1.81E-5 [2], [4]
3s–16p	9.385E-6	8.940E-6	15.5E-6 [2], [4]
3s–17p	8.588E-6	7.330E-6	12.39E-6 [2], [4]
3s–18p	7.503E-6	6.040E-6	10.32E-6 [2], [4]
3s–19p	5.637E-6	5.090E-6	

References. [1] Laser-based Faraday rotation spectroscopy (Nawaz et al. 1992); [2] Rozhdestvensky's hook method (Filippov & Prokofjew 1929); [3] Dirac-Hartree-Fock calculations (Froese Fischer 2002); [4] Coulomb approximation (Anderson & Zilitis 1964).

Their results disagree more strongly with our calculations and the measurements by Nawaz et al. (1992).

While the theoretical publications report f-values, most experimental studies measured the radiative lifetimes. However, f-values can be extracted from the reported lifetimes in a way similar to that used in our previous work (Civiš et al. 2010). In our comparison, we used QDT to calculate the ratios between f-values. These ratios are used to determine the absolute f-values from previously published experimental or theoretical lifetimes of the $3p_{\frac{1}{2},\frac{3}{2}}$, $4p_{\frac{1}{2},\frac{3}{2}}$ and $4d_{\frac{3}{2}}$ levels. Table 5 compares several QDT calculated f-values with f-values extracted from experimental and theoretical lifetimes. The overall agreement of our QDT calculation with the experimental values is not worse than that of other theoretical values given in the last column of Table 5.

Tables 3–5 show that the QDT calculations agree well with other methods. Table 6 presents the oscillator strength and the transition probability for each transition between the observed Na I states. Except where noted, the Ritz wavenumbers ν and air wavelengths λ given in Table 6 were calculated using the energy levels given in Table 2. In some instances, the energy was taken from more accurate sources (Martin & Zalubas 1981; Juncar et al. 1981). Therefore, some wavenumbers presented in Tables 6 and 1 may be slightly different. To our knowledge, no dipole matrix elements have been reported for most of the Na I transitions listed in Table 6.

4. Conclusion

We report the results of an FTIR spectroscopy study of Na I transitions in the range of 700–7000 cm^{-1} (1.4–14 μm). Few spectra of Na I have been measured in this spectral range (Johansson 1961; Litzen 1970) and no laboratory measurements of metal spectra are known below 1800 cm^{-1} ($\lambda > 5.5$ μm). Although the recorded wavenumbers agree with previous laboratory measurements within the corresponding uncertainties, they only partially agree with the data from the ACE solar spectrum (Hase et al. 2010) and infrared spectral atlases of the Sun from NOAO (Wallace et al. 1996). Therefore, new laboratory spectroscopic measurements are needed for the proper interpretation of current and future astrophysical spectra in the infrared domain.

Table 5. Comparison of Na I oscillator strengths ($f \times 100$) with strengths obtained from previously published experimental or calculated lifetimes.

		Other sources	
Transition	Present work	Experiment	Theory
$3s_{\frac{1}{2}}$–$3p_{\frac{3}{2}}$	62.2	64.07 ± 0.09 [2]	64.4 [1]
		64.13 ± 0.14 [3]	63.1 [5]
		64.16 ± 0.06 [4]	64.7 [7]
$3s_{\frac{1}{2}}$–$3p_{\frac{1}{2}}$	31.1	32.01 ± 0.04 [2]	32.2 [1]
		31.99 ± 0.12 [6]	32.3 [7]
		31.81 ± 0.06 [8]	31.91 ± 0.12 [9]
$3s_{\frac{1}{2}}$–$4p_{\frac{3}{2}}$	0.883	0.962 ± 0.03 [10]	0.875 [1]
			0.926 [5]
			0.886 [7]
			0.881 ± 0.033 [11]
$3s_{\frac{1}{2}}$–$4p_{\frac{1}{2}}$	0.434	0.467 ± 0.014 [10]	0.431 [1]
			0.436 [7]
			0.437 ± 0.016 [11]
$4s_{\frac{1}{2}}$–$4p_{\frac{3}{2}}$	95.1	103 ± 3 [10]	94.3 [1]
			99.7 [5]
			95.4 [7]
			94.9 ± 3.5 [11]
$4s_{\frac{1}{2}}$–$4p_{\frac{1}{2}}$	47.5	51.1 ± 1.5 [10]	47.1 [1]
			47.7 [7]
			47.7 ± 1.8 [11]
$3d_{\frac{3}{2}}$–$4p_{\frac{3}{2}}$	1.96	2.13 ± 0.07 [10]	1.94 [1]
			2.05 [5]
			1.96 [7]
			1.95 ± 0.07 [11]
$3d_{\frac{5}{2}}$–$4p_{\frac{3}{2}}$	11.7	12.8 ± 0.4 [10]	11.6 [1]
			12.3 [5]
			11.8 [7]
			11.7 ± 0.4 [11]
$3d_{\frac{3}{2}}$–$4p_{\frac{1}{2}}$	9.75	10.5 ± 0.03 [10]	9.67 [1]
			9.78 [7]
			9.80 ± 0.37 [11]
$3p_{\frac{1}{2}}$–$4d_{\frac{3}{2}}$	9.64	10.1 ± 0.1 [12]	9.76 [1]
		9.82 ± 0.06 [13]	9.76 [5]
		9.56 ± 0.05 [14]	9.77 [7]
$3p_{\frac{3}{2}}$–$4d_{\frac{3}{2}}$	0.962	1.01 ± 0.01 [12]	0.974 [1]
		0.980 ± 0.006 [13]	0.974 [5]
		0.954 ± 0.005 [14]	0.975 [7]
$4p_{\frac{1}{2}}$–$4d_{\frac{3}{2}}$	94.4	98.7 ± 1 [12]	95.5 [1]
		96.1 ± 0.6 [13]	95.5 [5]
		93.6 ± 0.5 [14]	95.6 [7]
$4p_{\frac{3}{2}}$–$4d_{\frac{3}{2}}$	9.45	9.89 ± 0.1 [12]	9.57 [1]
		9.63 ± 0.06 [13]	9.57 [5]
		9.37 ± 0.05 [14]	9.58 [7]

References. [1] Calculations by model potential method (Miculis & Meyer 2005); [2] beam-gas-laser spectroscopy (Volz et al. 1996); [3] precision spectroscopy on an optically prepared sample of ultracold, two-level atoms (Oates et al. 1996); [4] molecular spectroscopy of the Na_2 purely long-range O_g^- state (Jones et al. 1996); [5] numerical Coulomb approximation (Lindgård & Nielsen 1977); [6] measurements by molecular beam method (Tiemann et al. 1996); [7] realistic calculations including the core polarization, spin-orbit interaction, and blackbody radiation (Theodosiou 1984); [8] observing the decay in flight of laser-excited atoms in a fast atomic beam (Gaupp et al. 1982); [9] multiconfiguration Hartree-Fock calculations (Carlsson et al. 1992); [10] detecting the time-resolved fluorescence from the directly populated levels by the delayed-coincidence technique (Marek 1977); [11] multiconfiguration Hartree-Fock calculations (Jönsson et al. 1996); [12] measurements by stepwise excitation of a fast ion beam (Kandela 1984); [13] direct oscillography of the time dependence of light emitted from Na atoms, excited by short pulses of electrons (Karstensen & Schramm 1966); [14] time resolved observations of the fluorescence radiation after stepwise excitation by two pulsed dye lasers (Kaiser 1975).

The recorded spectra allowed us to extract the excitation energies of the 7h, 6h, and 6g states of Na I for which only theoretical predictions were available. These predictions were calculated by extrapolation from the higher nh and ng levels with $n \geq 13$ (Dyubko et al. 1997). The present study yielded more accurate energies for the 4s, 4p, 5p, 6p, 4f, 5f, and 5g levels of Na I (Risberg 1956; Johansson 1961; Litzen 1970; Arqueros 1988). For instance, the NIST energies of $4f_{\frac{5}{2},\frac{7}{2}}$ levels were reported a half century ago (Johansson 1961) without fine-structure resolution.

The f-values calculated using the quantum-defect theory approximation were presented for all transitions involving the

Table 6. QDT-calculated transition dipole moments for the observed transitions between Na I levels.

Transition i–k	Lower level (cm^{-1})	Upper level (cm^{-1})	ν (cm^{-1})	λ (nm)	$\log(g_i f_{ik})$	f_{ik}	A_{ki} (s^{-1})
$5d_{\frac{3}{2}}$–$6p_{\frac{3}{2}}$	37 036.772*	37 297.622	260.85	38 325.8	−1.50	5.59×10^{-2}	2.54×10^{3}
$5d_{\frac{3}{2}}$–$6p_{\frac{1}{2}}$	37 036.772*	37 297.622	260.85	38 325.8	+0.110	2.79×10^{-1}	2.54×10^{4}
$5d_{\frac{5}{2}}$–$6p_{\frac{3}{2}}$	37 036.752*	37 297.622	260.87	38 322.8	+0.698	3.35×10^{-1}	2.28×10^{4}
$4d_{\frac{3}{2}}$–$5p_{\frac{1}{2}}$	34 548.764*	35 040.387	491.623	20 335.2	−0.269	1.91×10^{-1}	6.14×10^{4}
$4d_{\frac{3}{2}}$–$5p_{\frac{3}{2}}$	34 548.764*	35 042.862	494.098	20 233.4	−1.88	3.83×10^{-2}	6.23×10^{3}
$4d_{\frac{5}{2}}$–$5p_{\frac{3}{2}}$	34 548.729*	35 042.862	494.133	20 232.0	+0.322	2.30×10^{-1}	5.61×10^{4}
$6p_{\frac{3}{2}}$–$7s_{\frac{1}{2}}$	37 297.622	38 012.042*	714.42	13 993.6	+0.860	5.91×10^{-1}	4.02×10^{5}
$6p_{\frac{1}{2}}$–$7s_{\frac{1}{2}}$	37 297.622	38 012.042*	714.42	13 993.6	+0.167	5.91×10^{-1}	2.01×10^{5}
$6g_{\frac{9}{2}}$–$7h_{\frac{9}{2}}$	38 400.865	39 209.681	808.786	12 361.2	−1.28	2.78×10^{-2}	1.21×10^{4}
$6g_{\frac{9}{2}}$–$7h_{\frac{11}{2}}$	38 400.865	39 209.681	808.786	12 361.2	+2.71	1.50	5.46×10^{5}
$6g_{\frac{7}{2}}$–$7h_{\frac{9}{2}}$	38 400.865	39 209.681	808.786	12 361.2	+2.50	1.53	5.34×10^{5}
$6s_{\frac{1}{2}}$–$6p_{\frac{3}{2}}$	36 372.618*	37 297.622	925.012	10 807.7	+1.12	1.53	4.38×10^{5}
$6s_{\frac{1}{2}}$–$6p_{\frac{1}{2}}$	36 372.618*	37 297.622	925.012	10 807.7	+0.428	7.67×10^{-1}	4.38×10^{5}
$6p_{\frac{3}{2}}$–$6d_{\frac{5}{2}}$	37 297.622	38 387.255*	1089.633	9174.90	+1.44	1.05	5.55×10^{5}
$6p_{\frac{3}{2}}$–$6d_{\frac{3}{2}}$	37 297.622	38 387.268*	1089.646	9174.79	−0.759	1.17×10^{-1}	9.25×10^{4}
$6p_{\frac{1}{2}}$–$6d_{\frac{3}{2}}$	37 297.622	38 387.268*	1089.646	9174.79	+0.850	1.17	4.63×10^{5}
$3d_{\frac{3}{2}}$–$4p_{\frac{1}{2}}$	29 172.887*	30 266.991	1094.097	9137.46	−0.942	9.75×10^{-2}	1.56×10^{5}
$3d_{\frac{3}{2}}$–$4p_{\frac{3}{2}}$	29 172.887*	30 272.586	1099.699	9090.92	−2.55	1.96×10^{-2}	1.58×10^{4}
$3d_{\frac{5}{2}}$–$4p_{\frac{3}{2}}$	29 172.837*	30 272.586	1099.744	9090.55	−0.354	1.17×10^{-1}	1.42×10^{5}
$5f_{\frac{7}{2}}$–$6d_{\frac{5}{2}}$	37 057.658	38 387.255*	1329.597	7519.03	−1.53	2.70×10^{-2}	4.25×10^{4}
$5f_{\frac{5}{2}}$–$6d_{\frac{5}{2}}$	37 057.658	38 387.255*	1329.597	7519.03	−4.53	1.80×10^{-3}	2.13×10^{3}
$5f_{\frac{5}{2}}$–$6d_{\frac{3}{2}}$	37 057.658	38 387.268*	1329.61	7518.95	−1.89	2.52×10^{-2}	4.46×10^{4}
$5p_{\frac{3}{2}}$–$6s_{\frac{1}{2}}$	35 042.862	36 372.618*	1329.751	7518.16	+0.592	4.52×10^{-1}	1.07×10^{6}
$5p_{\frac{1}{2}}$–$6s_{\frac{1}{2}}$	35 040.387	36 372.618*	1332.218	7504.23	−0.103	4.51×10^{-1}	5.34×10^{5}
$5g_{\frac{9}{2}}$–$6h_{\frac{9}{2}}$	37 059.497	38 401.148	1341.651	7451.47	−1.17	3.11×10^{-2}	3.74×10^{4}
$5g_{\frac{9}{2}}$–$6h_{\frac{11}{2}}$	37 059.497	38 401.148	1341.651	7451.47	+2.82	1.68	1.68×10^{6}
$5g_{\frac{7}{2}}$–$6h_{\frac{9}{2}}$	37 059.497	38 401.148	1341.651	7451.47	+2.62	1.71	1.65×10^{6}
$5f_{\frac{7}{2}}$–$6g_{\frac{9}{2}}$	37 057.658	38 400.865	1343.194	7442.91	+2.22	1.15	1.11×10^{6}
$5f_{\frac{7}{2}}$–$6g_{\frac{7}{2}}$	37 057.658	38 400.865	1343.194	7442.91	−1.33	3.29×10^{-2}	3.95×10^{4}
$5f_{\frac{5}{2}}$–$6g_{\frac{7}{2}}$	37 057.658	38 400.865	1343.194	7442.91	+1.96	1.18	1.07×10^{6}
$5s_{\frac{1}{2}}$–$5p_{\frac{1}{2}}$	33 200.673*	35 040.387	1839.707	5434.17	+0.222	6.24×10^{-1}	1.41×10^{6}
$5s_{\frac{1}{2}}$–$5p_{\frac{3}{2}}$	33 200.673*	35 042.862	1842.185	5426.86	+0.916	1.25	1.41×10^{6}
$5p_{\frac{3}{2}}$–$5d_{\frac{5}{2}}$	35 042.862	37 036.752*	1993.867	5014.01	+1.34	9.50×10^{-1}	1.68×10^{6}
$5p_{\frac{3}{2}}$–$5d_{\frac{3}{2}}$	35 042.862	37 036.772*	1993.91	5013.90	−0.858	1.06×10^{-1}	2.80×10^{5}
$5p_{\frac{1}{2}}$–$5d_{\frac{3}{2}}$	35 040.387	37 036.772*	1996.353	5007.77	+0.742	1.05	1.40×10^{6}
$5g_{\frac{9}{2}}$–$7h_{\frac{9}{2}}$	37 059.497	39 209.681	2150.197	4649.47	−3.15	4.30×10^{-3}	1.32×10^{4}
$5g_{\frac{9}{2}}$–$7h_{\frac{11}{2}}$	37 059.497	39 209.681	2150.197	4649.47	+0.842	2.32×10^{-1}	5.96×10^{5}
$5g_{\frac{7}{2}}$–$7h_{\frac{9}{2}}$	37 059.497	39 209.681	2150.197	4649.47	+0.636	2.36×10^{-1}	5.83×10^{5}
$4f_{\frac{7}{2}}$–$5d_{\frac{5}{2}}$	34 586.897	37 036.752*	2449.855	4080.76	−2.49	1.04×10^{-2}	5.56×10^{4}
$4f_{\frac{5}{2}}$–$5d_{\frac{5}{2}}$	34 586.893	37 036.752*	2449.859	4080.75	−5.48	6.94×10^{-4}	2.78×10^{3}
$4f_{\frac{5}{2}}$–$5d_{\frac{3}{2}}$	34 586.893	37 036.772*	2449.879	4080.72	−2.84	9.72×10^{-3}	5.84×10^{4}
$4f_{\frac{7}{2}}$–$5g_{\frac{9}{2}}$	34 586.897	37 059.497	2472.603	4043.22	+2.35	1.31	4.27×10^{6}
$4f_{\frac{7}{2}}$–$5g_{\frac{7}{2}}$	34 586.897	37 059.497	2472.603	4043.22	−1.21	3.74×10^{-2}	1.52×10^{5}
$4f_{\frac{5}{2}}$–$5g_{\frac{7}{2}}$	34 586.893	37 059.497	2472.603	4043.22	+2.09	1.35	4.12×10^{6}
$4d_{\frac{3}{2}}$–$5f_{\frac{5}{2}}$	34 548.764*	37 057.658	2508.894	3984.73	+1.24	8.62×10^{-1}	2.41×10^{6}
$4d_{\frac{5}{2}}$–$5f_{\frac{7}{2}}$	34 548.729*	37 057.658	2508.928	3984.68	+1.59	8.21×10^{-1}	2.59×10^{6}
$4d_{\frac{5}{2}}$–$5f_{\frac{5}{2}}$	34 548.729*	37 057.658	2508.928	3984.68	−1.40	4.11×10^{-2}	1.72×10^{5}
$4p_{\frac{3}{2}}$–$5s_{\frac{1}{2}}$	30 272.586	33 200.673*	2928.083	3414.27	+0.215	3.10×10^{-1}	3.55×10^{6}
$4p_{\frac{1}{2}}$–$5s_{\frac{1}{2}}$	30 266.991	33 200.673*	2933.671	3407.77	−0.478	3.10×10^{-1}	1.78×10^{6}
$5p_{\frac{3}{2}}$–$7s_{\frac{1}{2}}$	35 042.862	38 012.042*	2969.160	3367.04	−2.07	3.17×10^{-2}	3.73×10^{5}
$5p_{\frac{1}{2}}$–$7s_{\frac{1}{2}}$	35 040.387	38 012.042*	2971.655	3364.21	−2.76	3.18×10^{-2}	1.87×10^{5}
$5p_{\frac{3}{2}}$–$6d_{\frac{5}{2}}$	35 042.862	38 387.255*	3344.378	2989.28	−0.478	1.55×10^{-1}	7.72×10^{5}
$5p_{\frac{3}{2}}$–$6d_{\frac{3}{2}}$	35 042.862	38 387.268*	3344.406	2989.25	−2.68	1.72×10^{-2}	1.29×10^{5}
$5p_{\frac{1}{2}}$–$6d_{\frac{3}{2}}$	35 040.387	38 387.268*	3346.866	2987.06	−1.07	1.72×10^{-1}	6.44×10^{5}

Table 6. continued.

Transition i–k	Lower level (cm^{-1})	Upper level (cm^{-1})	ν (cm^{-1})	λ (nm)	$\log(g_i f_{ik})$	f_{ik}	A_{ki} (s^{-1})
$4f_{\frac{7}{2}}$–$6d_{\frac{5}{2}}$	34 586.897	38 387.255*	3800.358	2630.61	−4.21	1.85×10^{-3}	2.38×10^{4}
$4f_{\frac{5}{2}}$–$6d_{\frac{5}{2}}$	34 586.893	38 387.255*	3800.362	2630.61	−7.20	1.24×10^{-4}	1.19×10^{3}
$4f_{\frac{5}{2}}$–$6d_{\frac{3}{2}}$	34 586.893	38 387.268*	3800.375	2630.60	−4.57	1.73×10^{-3}	2.50×10^{4}
$4f_{\frac{7}{2}}$–$6g_{\frac{9}{2}}$	34 586.897	38 400.865	3813.968	2621.23	+0.353	1.78×10^{-1}	1.38×10^{6}
$4f_{\frac{7}{2}}$–$6g_{\frac{7}{2}}$	34 586.897	38 400.865	3813.968	2621.23	−3.20	5.08×10^{-3}	4.93×10^{4}
$4f_{\frac{5}{2}}$–$6g_{\frac{7}{2}}$	34 586.893	38 400.865	3813.972	2621.22	+0.0935	1.83×10^{-1}	1.33×10^{6}
$5s_{\frac{1}{2}}$–$6p_{\frac{3}{2}}$	33 200.673*	37 297.622	4096.949	2440.17	−2.50	4.12×10^{-2}	2.31×10^{5}
$5s_{\frac{1}{2}}$–$6p_{\frac{1}{2}}$	33 200.673*	37 297.622	4096.949	2440.17	−3.19	2.06×10^{-2}	2.31×10^{5}
$4p_{\frac{3}{2}}$–$4d_{\frac{5}{2}}$	30 272.586	34 548.729*	4276.126	2337.93	+1.22	8.51×10^{-1}	6.92×10^{6}
$4p_{\frac{3}{2}}$–$4d_{\frac{3}{2}}$	30 272.586	34 548.764*	4276.178	2337.90	−0.973	9.45×10^{-2}	1.15×10^{6}
$4p_{\frac{1}{2}}$–$4d_{\frac{3}{2}}$	30 266.991	34 548.764*	4281.759	2334.85	+0.636	9.44×10^{-1}	5.77×10^{6}
$4s_{\frac{1}{2}}$–$4p_{\frac{1}{2}}$	25 740.013	30 266.991	4526.968	2208.38	−0.0513	4.75×10^{-1}	6.49×10^{6}
$4s_{\frac{1}{2}}$–$4p_{\frac{3}{2}}$	25 740.013	30 272.586	4532.568	2205.65	+0.643	9.51×10^{-1}	6.51×10^{6}
$3d_{\frac{3}{2}}$–$4f_{\frac{5}{2}}$	29 172.887*	34 586.893	5414.005	1846.56	+1.40	1.01	1.31×10^{7}
$3d_{\frac{5}{2}}$–$4f_{\frac{5}{2}}$	29 172.837*	34 586.893	5414.06	1846.54	−1.25	4.79×10^{-2}	9.37×10^{5}
$3d_{\frac{5}{2}}$–$4f_{\frac{7}{2}}$	29 172.837*	34 586.897	5414.063	1846.54	+1.75	9.59×10^{-1}	1.41×10^{7}
$3d_{\frac{3}{2}}$–$5p_{\frac{1}{2}}$	29 172.887*	35 040.387	5867.5	1703.84	−7.47	1.42×10^{-4}	6.52×10^{3}
$3d_{\frac{3}{2}}$–$5p_{\frac{3}{2}}$	29 172.887*	35 042.862	5869.975	1703.12	−9.15	2.65×10^{-5}	6.10×10^{2}
$3d_{\frac{5}{2}}$–$5p_{\frac{3}{2}}$	29 172.837*	35 042.862	5870.025	1703.11	−6.95	1.59×10^{-4}	5.48×10^{3}
$4p_{\frac{3}{2}}$–$6s_{\frac{1}{2}}$	30 272.586	36 372.618*	6100.032	1638.89	−2.38	2.31×10^{-2}	1.15×10^{6}
$4p_{\frac{1}{2}}$–$6s_{\frac{1}{2}}$	30 266.991	36 372.618*	6105.627	1637.39	−3.07	2.32×10^{-2}	5.76×10^{5}
$4p_{\frac{3}{2}}$–$5d_{\frac{5}{2}}$	30 272.586	37 036.752*	6764.166	1477.97	−0.677	1.27×10^{-1}	2.59×10^{6}
$4p_{\frac{3}{2}}$–$5d_{\frac{3}{2}}$	30 272.586	37 036.772*	6764.186	1477.97	−2.88	1.41×10^{-2}	4.31×10^{5}
$4p_{\frac{1}{2}}$–$5d_{\frac{3}{2}}$	30 266.991	37 036.772*	6769.781	1476.75	−1.27	1.41×10^{-1}	2.16×10^{6}
$4p_{\frac{3}{2}}$–$7s_{\frac{1}{2}}$	30 272.586	38 012.042*	7739.456	1291.73	−3.54	7.28×10^{-3}	5.82×10^{5}
$4p_{\frac{1}{2}}$–$7s_{\frac{1}{2}}$	30 266.991	38 012.042*	7745.051	1290.79	−4.23	7.30×10^{-3}	2.92×10^{5}
$3d_{\frac{3}{2}}$–$5f_{\frac{5}{2}}$	29 172.887*	37 057.658	7884.771	1267.92	−0.453	1.59×10^{-1}	4.41×10^{6}
$3d_{\frac{5}{2}}$–$5f_{\frac{7}{2}}$	29 172.837*	37 057.658	7884.821	1267.91	−0.0921	1.52×10^{-1}	4.72×10^{6}
$3d_{\frac{5}{2}}$–$5f_{\frac{5}{2}}$	29 172.837*	37 057.658	7884.821	1267.91	−3.09	7.59×10^{-3}	3.15×10^{5}
$4p_{\frac{3}{2}}$–$6d_{\frac{5}{2}}$	30 272.586	38 387.255*	8114.669	1232.00	−1.74	4.40×10^{-2}	1.29×10^{6}
$4p_{\frac{3}{2}}$–$6d_{\frac{3}{2}}$	30 272.586	38 387.268*	8114.682	1232.00	−3.94	4.88×10^{-3}	2.15×10^{5}
$4p_{\frac{1}{2}}$–$6d_{\frac{3}{2}}$	30 266.991	38 387.268*	8120.277	1231.15	−2.32	4.89×10^{-2}	1.08×10^{6}
$3d_{\frac{3}{2}}$–$6p_{\frac{3}{2}}$	29 172.887*	37 297.622	8124.735	1230.47	−10.8	4.86×10^{-6}	2.14×10^{2}
$3d_{\frac{3}{2}}$–$6p_{\frac{1}{2}}$	29 172.887*	37 297.622	8124.735	1230.47	−9.24	2.43×10^{-5}	2.14×10^{3}
$3d_{\frac{5}{2}}$–$6p_{\frac{3}{2}}$	29 172.837*	37 297.622	8124.785	1230.47	−8.65	2.91×10^{-5}	1.93×10^{3}
$4s_{\frac{1}{2}}$–$5p_{\frac{1}{2}}$	25 740.013	35 040.387	9300.374	1074.93	−3.69	1.25×10^{-2}	7.22×10^{5}
$4s_{\frac{1}{2}}$–$5p_{\frac{3}{2}}$	25 740.013	35 042.862	9302.849	1074.65	−2.98	2.53×10^{-2}	7.30×10^{5}
$4s_{\frac{1}{2}}$–$6p_{\frac{3}{2}}$	25 740.013	37 297.622	11 557.609	864.993	−4.59	5.07×10^{-3}	2.26×10^{5}
$4s_{\frac{1}{2}}$–$6p_{\frac{1}{2}}$	25 740.013	37 297.622	11 557.609	864.993	−5.28	2.54×10^{-3}	2.26×10^{5}

Notes. The energy levels are taken from Table 2 except for those with an asterisk, which are taken from Martin & Zalubas (1981); Juncar et al. (1981). The air wavelengths are specified.

observed Na I levels. The approximation technique compares well with transition probabilities and oscillator strengths measured in other works (Miculis & Meyer 2005; Nawaz et al. 1992).

Acknowledgements. This work was financially supported by the Grant Agency of the Academy of Sciences of the Czech Republic (grant No. IAA400400705), by the Ministry of Finance of the Czech Republic (Project ECPF:049/4V) and the Ministry of Education, Youth, and Sports of the Czech Republic (grant No. LM2010014).

References

Anderson, E. M., & Zilitis, V. A. 1964, Opt. Spectrosk., 16, 177
Andrievsky, S. M., Egorova, I. A., Korotin, S. A., & Burnage, R. 2002, A&A, 389, 519
Aragon, C., & Aguilera, J. A. 2008, Spectrochim. Acta, 63, 893
Arqueros, F. 1988, Opt. Commun., 67, 341
Babánková, D., Civiš, S., & Juha, L. 2006, Prog. Quant. Electron., 30, 75
Barthélemy, O., Margot, J., Chaker, M., et al. 2005, Spectrochim. Acta, 60, 905
Biémont, E. 1994, in Infrared Solar Physics, ed. D. M. Rabin, J. T. Jefferies, & C. Lindsey, IAU Symp., 154
Carlsson, J., Jönsson, P., Sturesson, L., & Fischer, C. F. 1992, Phys. Scr., 46, 394
Chang, E. S., & Schoenfeld, W. G. 1991, ApJ, 383, 450
Charbonneau, D., Brown, T. M., Noyes, R. W., & Gilliland, R. L. 2002, ApJ, 568, 377
Chernov, V., Manakov, N., & Starace, A. 2000, Eur. Phys. J. D, 8, 347
Chernov, V. E., Dorofeev, D. L., Kretinin, I. Y., & Zon, B. A. 2005a, Phys. Rev. A, 71, 022505
Chernov, V. E., Dorofeev, D. L., Kretinin, I. Y., & Zon, B. A. 2005b, J. Phys. B, 38, 2289
Civiš, S., Matulková, I., Cihelka, J., et al. 2010a, Phys. Rev. A, 81, 012510

Civiš, S., Matulková, I., Cihelka, J., et al. 2010b, Phys. Rev. A, 82, 022502
Civiš, S., Matulková, I., Cihelka, J., et al. 2011a, J. Phys. B, 44, 105002
Civiš, S., Matulková, I., Cihelka, J., et al. 2011b, J. Phys. B, 44, 025002
Dyubko, S., Efremov, V., Podnos, S., Sun, X., & MacAdam, K. B. 1997, J. Phys. B, 30, 2345
Filippov, A., & Prokofjew, W. 1929, Z. Phys., 56, 458
Froese Fischer, C. 2002, The MCHF/MCDHF Collection, non-orthogonal B-spline CI caclulations, http://atoms.vuse.vanderbilt.edu
Gaupp, A., Kuske, P., & Andrä, H. J. 1982, Phys. Rev. A, 26, 3351
Giacomo, A. D., Shakhatov, V., & Pascale, O. D. 2001, Spectrochim. Acta Part B: Atomic Spectrosc., 56, 753
Gomes, A., Aubreton, A., Gonzalez, J. J., & Vacquié, S. 2004, J. Phys. D, 37, 689
Grava, C., Schneider, N. M., & Barbieri, C. 2010, in Galileo's Medicean Moons: Their Impact on 400 Years of Discovery, ed. C. Barbieri, S. Chakrabarti, M. Coradini, & M. Lazzarin, IAU Symp. Proc. Ser., 269, 224
Grevesse, N., & Noels, A. 1994, Phys. Scr. T, 51, 47
Hase, F., Wallace, L., McLeod, S. D., Harrison, J. J., & Bernath, P. F. 2010, J. Quant. Spectrosc. Radiat. Trans., 111, 521
Jensen, A. G., Redfield, S., Endl, M., et al. 2011, ApJ, 743, 203
Johansson, I. 1961, Ark. Fys., 20, 135
Johansson, S. 2005, in High Resolution Infrared Spectroscopy In Astronomy, Proceedings, ed. H. U. Kaufl, R. Siebenmorgen, & A. Moorwood, ESO Astrophysics Symposia, ESO (Germany: Springer-Verlag Berlin), 62
Jones, K. M., Julienne, P. S., Lett, P. D., et al. 1996, Europhys. Lett., 35, 85
Jönsson, P., Ynnerman, A., Froese Fischer, C., Godefroid, M. R., & Olsen, J. 1996, Phys. Rev. A, 53, 4021
Jorissen, A. 2004, Phys. Scr. T, 112, 73
Juncar, P., Pinard, J., Hamon, J., & Chartier, A. 1981, Metrologia, 17, 77
Kaiser, D. 1975, Phys. Lett. A, 51, 375
Kandela, S. A. 1984, Appl. Opt., 23, 2152
Karstensen, F., & Schramm, J. 1966, Z. Phys., 195, 370
Kawaguchi, K., Sanechika, N., Nishimura, Y., et al. 2008, Chem. Phys. Lett., 463, 38
Kelleher, D. E., & Podobedova, L. I. 2008, J. Phys. Chem. Ref. Data, 37, 267
Kerber, F., Nave, G., Sansonetti, C. J., & Bristow, P. 2009, Phys. Scr. T, 134, 014007
Khalil, A., & Sreenivasan, N. 2005, Laser Phys. Lett., 2, 445
Lednev, V. N., & Pershin, S. M. 2008, Laser Phys., 18, 850
Lee, W.-B., Wu, J.-Y., Lee, Y.-I., & Sneddon, J. 2004, Appl. Spectrosc. Rev., 39, 27
Lee, D.-W., Kim, S. J., Lee, D.-H., Jin, H., & Kim, K.-S. 2011, J. Geophys. Res., 116, 7213
Lindgård, A., & Nielsen, S. E. 1977, At. Data Nucl. Data Tables, 19, 533
Litzen, U. 1970, Phys. Scr., 1, 253
Lobel, A. 2011, Can. J. Phys., 89, 395
Marek, J. 1977, J. Phys. B, 10, L325
Martin, W. C., & Zalubas, R. 1981, J. Phys. Chem. Ref. Data, 10, 153
Matta, M., Smith, S., Baumgardner, J., et al. 2009, Icarus, 204, 409
Meléndez, J., & Barbuy, B. 1999, ApJS, 124, 527
Miculis, K., & Meyer, W. 2005, J. Phys. B, 38, 2097
Mouawad, N., Burger, M. H., Killen, R. M., et al. 2011, Icarus, 211, 21
Nawaz, M., Farooq, W. A., & Connerade, J.-P. 1992, J. Phys. B, 25, 5327
Nilsson, H. 2009, Phys. Scr. T, 134, 014009
Oates, C. W., Vogel, K. R., & Hall, J. L. 1996, Phys. Rev. Lett., 76, 2866
O'Donovan, F. T., Charbonneau, D., Harrington, J., et al. 2010, ApJ, 710, 1551
OPUS 2010, Opus Spectroscopy Software, http://www.brukeroptics.com/opus.html
Pickering, J. C. 1999, Phys. Scr. T, 83, 27
Pickering, J., Blackwell-Whitehead, R., Thorne, A., Ruffoni, M., & Holmes, C. 2011, Can. J. Phys., 89, 387
Qi, H., Sun, Y., Liu, X., Hou, X., & Li, Y. 2007, Laser Phys. Lett., 4, 212
Radziemski, L. J., Fisher, K. J., Steinhaus, D. W., & Goldman, A. S. 1972, Comput. Phys. Commun., 3, 9
Ralchenko, Y., Kramida, A., Reader, J., & NIST ASD Team 2010, NIST Atomic Spectra Database, version 4.0
Redfield, S., Endl, M., Cochran, W. D., & Koesterke, L. 2008, ApJ, 673, L87
Risberg, P. 1956, Ark. Fys., 10, 583
Ryde, N. 2010, Astron. Nachr., 331, 433
Sansonetti, J. E. 2008, J. Phys. Chem. Ref. Data, 37, 1659
Spitoni, E., Recchi, S., & Matteucci, F. 2008, A&A, 484, 743
Sternberg, A., Gal-Yam, A., Simon, J. D., et al. 2011, Science, 333, 856
Taylor, K. T. 1995, TOPBASE (Opacity Project), http://cdsweb.u-strasbg.fr/topbase/topbase.html
Theodosiou, C. E. 1984, Phys. Rev. A, 30, 2881
Tiemann, E., Knöckel, H., & Richling, H. 1996, Z. Phys. D, 37, 323
Volz, U., Majerus, M., Liebel, H., Schmitt, A., & Schmoranzer, H. 1996, Phys. Rev. Lett., 76, 2862
Wahlgren, G. M. 2011, Can. J. Phys., 89, 345
Wallace, L., Livingston, W., Hinkle, K., & Bernath, P. 1996, ApJS, 106, 165
Wallace, L., Meyer, M. R., Hinkle, K., & Edwards, S. 2000, ApJ, 535, 325